# Cataract-associated mutant E107A of human γD-crystallin shows increased attraction to α-crystallin and enhanced light scattering

Priya R. Banerjee[a], Ajay Pande[a], Julita Patrosz[b,1], George M. Thurston[c], and Jayanti Pande[a,2]

[a]Department of Chemistry, and [b]Department of Biology, University at Albany, State University of New York, Albany, NY 12222; and [c]Department of Physics, Rochester Institute of Technology, Rochester, NY 14623

Edited by George B. Benedek, Massachusetts Institute of Technology, Cambridge, MA, and approved November 2, 2010 (received for review September 30, 2010)

**Several point mutations in human γD-crystallin (HGD) are now known to be associated with cataract. So far, the in vitro studies of individual mutants of HGD alone have been sufficient in providing plausible molecular mechanisms for the associated cataract in vivo. Nearly all the mutant proteins in solution showed compromised solubility and enhanced light scattering due to altered homologous γ–γ crystallin interactions. In sharp contrast, here we present an intriguing case of a human nuclear cataract-associated mutant of HGD—namely Glu107 to Ala (E107A), which is nearly identical to the wild type in structure, stability, and solubility properties, with one exception: Its pI is higher by nearly one pH unit. This increase dramatically alters its interaction with α-crystallin. There is a striking difference in the liquid–liquid phase separation behavior of E107A–α-crystallin mixtures compared to HGD–α-crystallin mixtures, and the light-scattering intensities are significantly higher for the former. The data show that the two coexisting phases in the E107A–α mixtures differ much more in protein density than those that occur in HGD–α mixtures, as the proportion of α-crystallin approaches that in the lens nucleus. Thus in HGD–α mixtures, the demixing of phases occurs primarily by protein type while in E107A–α mixtures it is increasingly governed by protein density. Analysis of these results suggests that the cataract due to the E107A mutation could result from the instability caused by the altered attractive interactions between dissimilar proteins —i.e., heterologous γ–α crystallin interactions—primarily due to the change in surface electrostatic potential in the mutant protein.**

The vertebrate lens contains three families of constituent proteins, the α-, β-, and γ-crystallins, closely packed such that the total protein concentration in the central region of the lens, i.e., nucleus, exceeds 400 mg/mL (1). Normally, the close protein packing ensures that short-range order is maintained within the fiber cell, such that fluctuations in the refractive index that cause light scattering are minimized, and the lens is transparent (2, 3). Disruption of short-range order associated with aging, altered environment, or mutations in crystallins can cause increased light scattering and cataract.

Cataract-associated mutations in the crystallin genes are known to occur in all three crystallin families (1, 4) and show a variety of phenotypes. Over the last decade, we have focused on the point mutations occurring in human γD-crystallin (HGD), a member of the γ-crystallin family expressed at high levels along with γC- and γS-crystallins in the human lens (5). By comparing the properties of several mutants of HGD in solution with those of the wild type, we have identified specific changes in the homologous (i.e., γ–γ interactions) that led to the formation of distinct condensed phases (6, 7) and accounted for the increased light scattering due to these mutations (8–13). These studies revealed a class of γ-crystallin mutations in which small changes to the protein surface were sufficient to bring about severe solubility changes, without unfolding the protein, and were in direct contrast to other mutations (i.e., other missense mutations, insertions, and splice mutations) that are accompanied by alterations in protein fold and stability (1, 14, 15).

Here we report on yet another cataract-associated mutation in HGD—the Glu107 to Ala (E107A) mutation—first reported in 2006 by Messina-Baas et al. (16) from genetic association studies. As in the case of the other mutants we have studied, the E107A mutant also shows minimal alterations in structure and stability. However, unlike the mutants described above, we find that the E107A mutation does not form a distinct condensed phase that could result in a measurable lowering of solubility—instead, it is soluble to protein concentrations upwards of 325 mg/mL just like HGD at pH 7. These data clearly suggested that despite the loss of a negative charge following the replacement of Glu107 with Ala, the γ–γ (homologous) interactions among the mutant protein molecules remain essentially unaltered relative to those in HGD. As expected, there is a difference in the isoelectric point (pI) between HGD and E107A with the pI of E107A being approximately one pH unit higher ($8.2 \pm 0.1$) than that of HGD ($7.2 \pm 0.1$). Because the net γ–γ interactions are essentially unaltered in E107A relative to HGD, the increase in pI raises the possibility of altered electrostatic interactions between E107A and other crystallins—for example, one with a lower pI. A likely candidate is α-crystallin, because it is negatively charged at physiological pH (17), and it is already known that interactions among α- and γ-crystallins are fine tuned for optimal packing and transparency, and small changes in such interactions lead to instability (18–22).

We therefore examined mixtures containing solutions of α-crystallin and either HGD or E107A, at compositions representing those in the young human lens and approaching those in the lens nucleus (23). Here we show that all the mixtures containing E107A and α-crystallin (E107A–α) consistently show higher light-scattering intensities relative to mixtures of HGD and α-crystallin (HGD–α) of identical composition. Furthermore, as the weight fraction of α-crystallin ($X_\alpha$) in E107A–α mixtures is raised incrementally from 0.2 to 0.5 (a value comparable to that in the lens nucleus) (24), the observed changes in the phase separation temperature ($T_{ph}$) and the tie lines of the mixtures are consistent with an increase in the attraction between E107A and α-crystallin (22).

Preliminary accounts of parts of this work were presented at the Association for Research in Vision and Ophthalmology annual meeting in Fort Lauderdale, FL, 2009, and the Biophysical Society annual meeting in San Francisco, 2010.

Author contributions: A.P., G.M.T., and J. Pande designed research; P.R.B., A.P., and J. Patrosz performed research; P.R.B., A.P., G.M.T., and J. Pande analyzed data; and P.R.B., A.P., G.M.T., and J. Pande wrote the paper.

The authors declare no conflict of interest.

This article is a PNAS Direct Submission.

See Commentary on page 437.

[1]Present address: Regeneron Pharmaceuticals, 745 Old Sawmill River Road, Tarrytown, NY 10591.

[2]To whom correspondence should be addressed. E-mail: jpande@albany.edu.

This article contains supporting information online at www.pnas.org/lookup/suppl/doi:10.1073/pnas.1014653107/-/DCSupplemental.

The E107A–α mixture with $X_\alpha = 0.5$ undergoes density-type phase separation, unlike all the HGD-α mixtures examined. Thus these data provide direct experimental evidence for the prediction of Dorsaz et al. (22) that an increase in the attractive interactions between the α- and γ-crystallins will make mixtures of these proteins unstable, tending toward density-driven phase separation, and can thereby contribute to cataract formation. This work also constitutes a prime example of a cataract-associated mutation that highlights the importance of heterologous protein–protein interactions optimized to maintain transparency and how changes in these interactions can lead to instability and opacity of the human lens. We note here that the role of heterologous protein–protein interactions between HGD and βB1 crystallins in affecting thermodynamic stability has also been studied recently (25). In analogy to our present work, one might expect cataractogenic mutations in the future that impact stability primarily through their effects on, for example, the γ–β interactions.

## Results

**Comparison of the Structures of HGD and E107A.** Near- and far-UV CD studies: In Fig. S1 we compare the CD spectra of HGD and E107A in the near-UV (Fig. S1*A*) and far-UV (Fig. S1*B*) regions. The near-UV CD data show that the tertiary structures of the two proteins are virtually indistinguishable, indicating that the substitution of Glu107 with Ala does not alter the protein fold. This is also true for the secondary structure represented by the far-UV spectra. Both proteins have far-UV CD profiles typical of predominantly β-sheet-containing proteins, with a minor increase in the negative ellipticity bands for E107A but well within the differences observed in other highly homologous γ-crystallins (26). Therefore, we conclude from these studies that the secondary and tertiary structures of HGD do not undergo any significant change upon mutation.

**Fluorescence Studies.** ***Tryptophan fluorescence.*** The tryptophan fluorescence emission spectra are shown in Fig. S2*A*. γ-crystallins contain four buried tryptophan residues, two in each domain, which are excellent reporters of the overall structural integrity of the protein (27). Fig. S2*A* shows that the fluorescence emission spectra for HGD and E107A are comparable, and the intensities are almost equally quenched for both proteins. The $\lambda_{max}$ values for HGD and E107A of 327 and 326 nm, respectively, are typical of tryptophan residues buried within the hydrophobic core. The two proteins also show nearly identical fluorescence spectra when unfolded with guanidinium hydrochloride (Gdn.HCl), shown in Fig. S2*A*, again attesting to their structural similarity.

***Bis-ANS and Nile Red Fluorescence to determine surface hydrophobicity.*** The surface hydrophobicities of HGD and E107A were determined using two well-tested fluorescent probes, the negatively charged Bis-ANS and the uncharged Nile Red. Based on the fluorescence changes (Fig. S2*B*), the Bis-ANS data show a small increase in the net surface hydrophobicity for E107A compared to HGD, while Nile Red does not. Because Bis-ANS is known to be a more sensitive probe for surface hydrophobicity compared to Nile Red (28), this difference is not surprising. The slight increase in surface hydrophobicity is consistent with the substitution of Glu by Ala in the mutant. We note however that because Bis-ANS is negatively charged and Nile Red is neutral, the difference in fluorescence could be due to the stronger electrostatic interactions between the negatively charged Bis-ANS and E107A, which is more positively charged than HGD. Thus the mutant may only have a marginally higher surface hydrophobicity relative to the wild-type protein.

**Thermal and Chemical Denaturation.** Thermal stabilities of the two proteins were measured by the loss of ellipticity at 290 nm in the near-UV CD spectrum, in 0.1 M sodium phosphate buffer, pH 7 (Fig. S3). The midpoint of the transition corresponds to the melting temperature ($T_m$) for each protein. Fig. S3 shows that both proteins unfold in an apparently single step without the formation of a stable intermediate, and the respective $T_m$ values differ by less than 2 ° (≅79.3 °C for HGD and ≅77.7 °C for E107A). The apparent reduction in $T_m$ is not significant because small variations in $T_m$ (2–4 °C) are typical even among members of the γ-crystallin family in their native state (12, 27). The inset of Fig. S3 shows chemical unfolding data using Gdn.HCl as a denaturant and recorded as a change in the tryptophan fluorescence spectra. Because all four tryptophan residues in HGD are significantly quenched, the unfolding process can be reliably monitored as an increase in the tryptophan fluorescence intensity around 350 nm with a corresponding decrease around 320 nm. The data in Fig. S3 show also that both wild-type and mutant unfold by an apparently single-step transition, just as in the case of thermal unfolding, with midpoint values of 3.54 M and 3.44 M Gdn.HCl for HGD and E107A, respectively. These data clearly suggest that the conformational stability of the mutant protein is comparable to that of the wild type.

**Isoelectric Focusing.** The first evidence for a clear distinction between HGD and E107A came from the measurement of the pI. Fig. 1 shows a representative isoelectric-focusing gel (IEF) for HGD and E107A with pI values of 7.3 and 8.1, respectively. Repeat runs yielded an average pI value of $7.2 \pm 0.1$ for HGD and $8.2 \pm 0.1$ for E107A. The increase in pI of approximately one pH unit confirms that there is an effective increase in overall positive charge in E107A relative to HGD. Therefore, except for the increase in pI, E107A appears similar in structure and stability to HGD.

We also found that the mutant protein could be concentrated to at least 325 mg/mL without the appearance of any condensed phase, just like HGD. Thus it became apparent that the homologous interactions between E107A molecules may not be the basis of cataract, in contrast to many other γ-crystallin mutants we reported earlier (8, 12, 13). However, the increase in pI of the mutant pointed to the possibility of altered interaction with α-crystallin, which is negatively charged at the physiological pH (17). Thurston and colleagues (20–22, 29) have been investigating the interactions between native α- and γ-crystallins and predicted that the strength of the γ–α interactions in the lens is optimized for transparency in a very narrow range, and deviations from this range would lead to instability and cataract. Their work provided the impetus for us to examine E107A–α interactions, and therefore we compared the thermodynamic properties of a series of mixtures containing either HGD or E107A and α-crystallin in

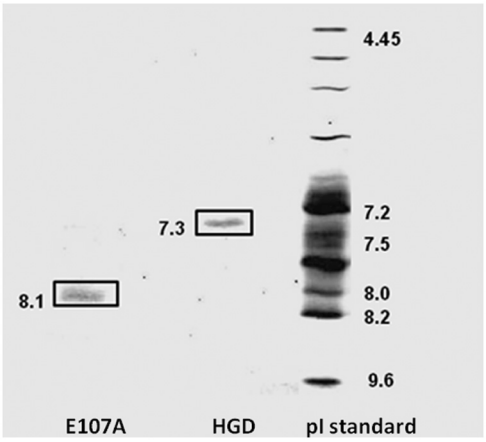


**Fig. 1.** Isoelectric-focusing gel for HGD and E107A. The Glu107 to Ala mutation causes an increment of approximately 1.0 pH unit in the pI of the protein.

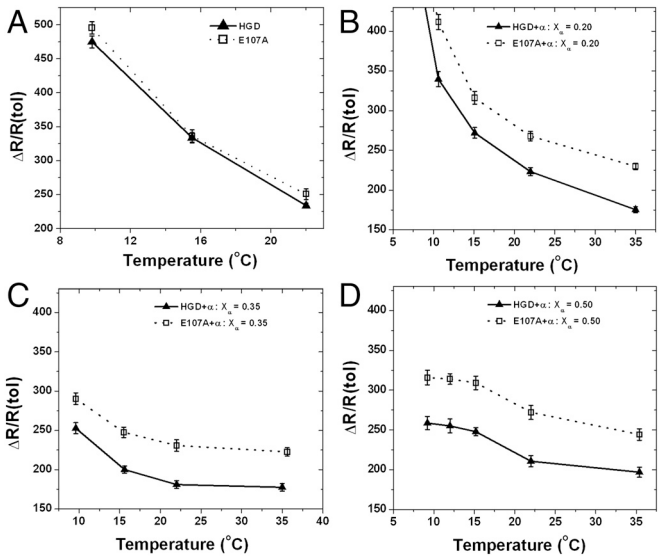


**Fig. 2.** Light-scattering efficiencies of HGD-α-crystallin (▲) and E107A–α-crystallin mixtures (□) at (*A*) weight fraction of α-crystallin, $X_\alpha = 0.0$ (pure proteins), (*B*) $X_\alpha = 0.2$, (*C*) $X_\alpha = 0.35$, and (*D*) $X_\alpha = 0.5$ as a function of temperature, at a total protein concentration of 265 mg/mL for pure proteins and 275 mg/mL for mixtures.

solution. The data, presented in this report, constitute remarkable developments in the molecular basis for lens opacity due to a human cataract-associated mutation.

**Light-Scattering Efficiencies of HGD–α and E107A–α Mixtures.** Light scattering is intimately associated with cataract disease, and all cataract-associated mutants of HGD show increased light scattering relative to the normal protein at appropriate concentrations (8, 12, 13). In Fig. 2 we compare the light-scattering efficiencies, expressed as excess Rayleigh ratios, of the pure proteins (Fig. 2*A*) as well as solutions containing mixtures (either HGD–α or E107A–α) at three different compositions ($X_\alpha = 0.2$, 0.35, and 0.5) at a total protein concentration of 275 mg/mL (Fig. 2 *B–D*). The light-scattering profiles of the two proteins, HGD and E107A alone, are nearly identical (Fig. 2*A*), further attesting to the similarity between the two proteins. However, in contrast, the data for the E107A–α mixtures show a nearly 25% increase in light scattering relative to the HGD–α mixtures at all three compositions ($X_\alpha = 0.20$, 0.35, and 0.50) and temperatures examined (10–35 °C). The difference in scattering efficiency between the two remains virtually independent of temperature and composition at $X_\alpha = 0.5$. As stated earlier, in terms of the composition, the mixtures at $X_\alpha = 0.5$ are comparable to that found in the lens nucleus (30). Thus, the light-scattering efficiencies for the E107A–α mixtures relative to the HGD–α mixtures at all the temperatures studied show inherently higher light-scattering profiles. Notably, as we approach the critical temperature for phase separation in each mixture (<10 °C), the difference in light-scattering efficiencies seems to be dominated by the instability due to the phase transition, which is clearly observed in Fig. 2*B* where the proportion of γ-crystallin is at a maximum in the mixture.

**Coexistence Curves of Pure HGD and E107A and of Mixtures.** Because coexistence curves provide a measure of the strength of protein–protein interactions (31), we measured liquid–liquid phase separation in solutions of pure γ-crystallins as well as in E107A–α and HGD–α mixtures. In Fig. 3 we compare the data for pure HGD and E107A (Fig. 3*A*) and several mixtures as a function of the weight fraction of α-crystallin (Fig. 3*B*) and total protein concentration (Fig. 3*C*). Again, as expected, the $T_{ph}$ values for the pure proteins are nearly identical and fall on the coexistence curve for HGD published earlier (8). Thus, the data in Fig. 3*A* confirm that the magnitude of the like–like (i.e., γ–γ) homologous interactions in E107A are nearly identical to those in HGD, despite the loss of a negative charge in E107A.

This behavior changes dramatically when we compare the liquid–liquid phase separation profiles of HGD–α and E107A–α mixtures. The coexistence curve (Fig. 3*B*) and the $T_{ph}$ profile (Fig. 3*C*) for E107A–α were suppressed relative to those for HGD–α. In *Discussion* we show how such a suppression of $T_{ph}$ is in fact expected to accompany an initial increase in γ–α attraction, based on previous work (22), and how such a change, together with the increase in light scattering well above $T_{ph}$ and the rotation of the tie lines toward density–density phase separation (see below) can all be consistent with an increase in E107A–α attraction over that of HGD–α. In *Appendix S1* we construct a mean-field model to help analyze the qualitative response of each measured quantity to changes in γ–α attraction strength. The model is also consistent with the inference of increased γ–α attraction in going from the HGD–α to the E107A–α mixtures.

**Tie Lines and Concentrations and Compositions of the Coexisting Phases in HGD–α and E107A–α Mixtures.** Next we examined the tie lines that join equilibrium protein compositions of the separated phases in HGD–α and E107A–α mixtures (Fig. 4). At 20% α-crystallin ($X_\alpha = 0.2$, Fig. 4*A*), the dense phase contains predominantly γ-crystallin and the dilute phase contains mostly α-crystallin, and the tie lines are essentially the same for both mixtures. These data are consistent with the measured tie lines of mixtures of bovine α- and γB-crystallins at low $X_\alpha$ values (21). As $X_\alpha$ increases to 0.35 (Fig. 4*B*), there is a noticeable counterclockwise rotation of the tie line for E107A–α, relative to that for HGD–α. The coun-

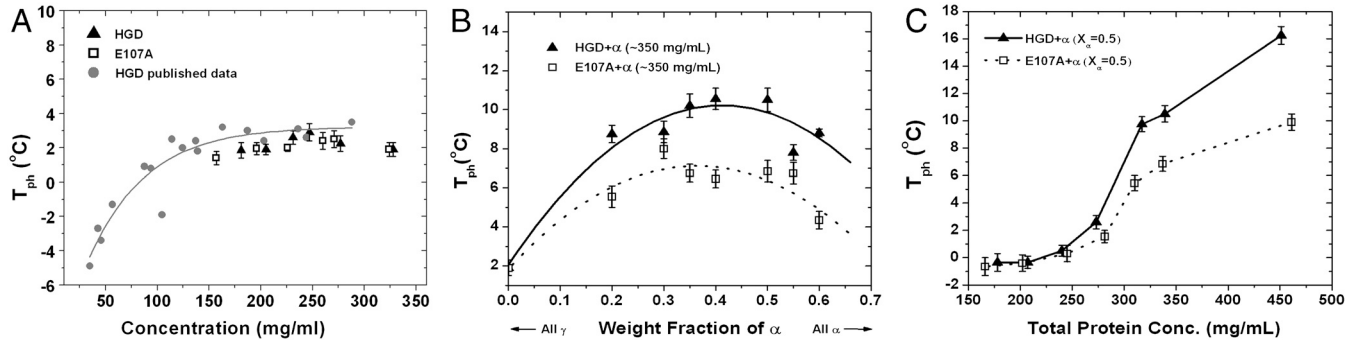


**Fig. 3.** (*A*) Liquid–liquid coexistence curves of pure HGD and E107A in 0.1 M phosphate buffer, pH 7.0, containing 20 mM DTT. The data obtained in the present study [HGD, (▲), E107A, (□)], are compared with the published HGD data (8) (filled gray circles). (*B*) Liquid–liquid coexistence curves of HGD–α and E107A–α mixtures as a function of $X_\alpha$ at a constant total protein concentration of approximately 350 mg/mL, 0.1 M phosphate buffer, pH 7.0, containing 20 mM DTT. The lines are shown as guides to the eye. (*C*) Change in the ($T_{ph}$) for HGD–α and E107A–α mixtures as a function of total protein concentration at $X_\alpha = 0.50$ in 0.1 M phosphate buffer, pH 7.0, containing 20 mM DTT. Lines drawn through the data in all the figures are merely guides to the eye.

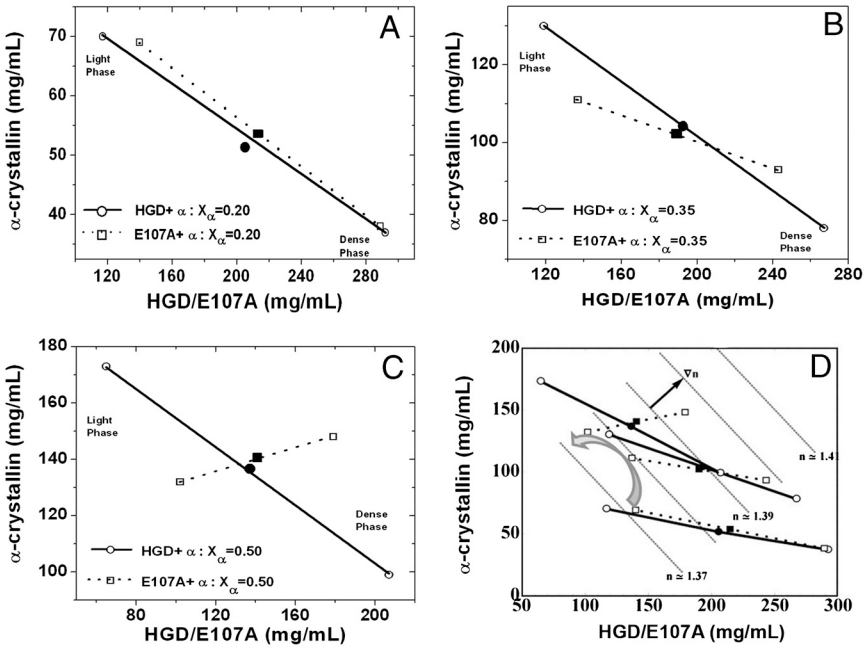


**Fig. 4.** Tie lines for the coexistence curves showing the compositions of the two phases of mixtures of HGD–α or E107A–α: (*A*) at $X_\alpha = 0.20$, (*B*) $X_\alpha = 0.35$, and (*C*) $X_\alpha = 0.50$, in 0.1 M phosphate buffer, pH 7.0, containing 20 mM DTT. In *D* all the tie lines are shown, along with the rotation of the tie lines for the E107A–α mixtures (curved arrow). The parallel dotted lines (in gray) are contours of constant refractive index, and the gradient of refractive index ($\nabla n$) is indicated by a small black arrow. Starting protein concentrations for each mixture is shown as a solid circle for HGD–α and a solid cube for E107A–α mixtures, respectively. The quench temperature for $X_\alpha = 0.2$ and 0.5 mixtures were 0.5 °C while that for $X_\alpha = 0.35$ was 0.8 °C.

terclockwise rotation is much more pronounced when $X_\alpha$ is further increased to 0.5 (Fig. 4*C*). Here, the tie line for E107A–α is nearly perpendicular to that of HGD–α, and the dense protein phase is enriched in both α- and γ-crystallins while the dilute phase is poor in both α- and γ-crystallins, while HGD–α at $X_\alpha = 0.5$ still shows more compositional phase separation. Thus as protein composition and concentration approach values comparable to those in the lens nucleus ($X_\alpha = 0.5$), demixing changes from being predominantly by "protein type" (HGD–α), toward "density-type" (E107A–α), a phenomenon analyzed by Dorsaz et al. (22). Fig. 4*D* shows the assembled tie line results with a backdrop of estimated refractive index contours. In Fig. S4*I* we present a three-dimensional view of the phase diagrams of the HGD–α and E107A–α ternary mixtures. In Fig. S4*II* we show the orientations of the tie lines at $X_\alpha = 0.5$ with respect to the refractive index gradient ($\nabla n$). The E107A–α tie line is approximately 30° from $\nabla n$, while the HGD–α tie line is 70° away (Fig. 4*D* and Fig. S4*II*). The relationship between the rotation of the tie lines, increased attractive E107A–α interactions, and the possible consequences for increased light scattering from E107A–α mixtures are discussed below and modeled mathematically in *Appendix S1*.

**Modeling Attractive Interactions Between HGD/E107A and α-crystallin.** We have computationally modeled the putative attractive interactions between E107A and α-crystallin, based on the high-resolution crystal structures of HGD (32) and truncated human αB-crystallin (HAB), respectively (33). These studies point out that the mutation in E107A could result in a distinct positive-potential surface patch that is likely to show attractive interactions with a large negative-potential patch present on the surface of HAB. We obtained an electrostatic interaction energy of −2.04 kcal/mol for the HGD–HAB interaction and −2.43 kcal/mol for the E107A–HAB interaction, representing a change in interaction energy that is consistent with stronger attractive interactions of E107A with α-crystallin. The details of the methods used, justification for the use of HAB to model bovine α-crystallin, results of the modeling, and corresponding discussion are presented in *Appendix S2*.

## Discussion

Our data show that the cataract-associated E107A mutant of HGD is a novel case where neither structure and stability, nor the stability of its aqueous solutions with respect to precipitation, is significantly compromised as a result of the mutation. The strong similarity in the coexistence curves of the two proteins indicates that the strength of the γ–γ interaction in the mutant is nearly identical to that in the wild-type protein. Therefore, we conclude that the molecular basis for lens opacity in this case cannot be attributed directly to the altered, homologous γ–γ interactions in the mutant.

The isoelectric-focusing data confirm an expected primary difference between the mutant and wild-type proteins by showing a pI increase of about one pH unit for E107A. Consistent with this increase, E107A will be more positively charged than HGD at physiological pH. Mapping the electrostatic potential on the protein surfaces revealed a positive-potential patch that includes residues Arg89, Arg115, and Arg169 in E107A, and that is clearly different from that in the wild type (Fig. S5 *A* and *B*).

It is known that α-crystallins are negatively charged at physiological pH (17), and it is only recently that Thurston and colleagues (20–22) have shown comprehensively that heterologous interactions between the α- and γ-crystallins are so delicately balanced that even slight (~0.5 $k_BT$) strengthening or weakening of such interactions could lead to instability in mixtures containing these proteins (22). Our comparison of the thermodynamic properties of mixtures of either HGD or E107A with α-crystallin at physiological pH, and at high concentrations comparable to those in the eye lens, provides significant experimental evidence to support their prediction for a cataract-associated mutant of HGD.

We now discuss how the (a) lowered $T_{ph}$ values, (b) enhanced protein density-type phase separation resulting in rotated tie lines, and (c) enhanced light scattering in the single-phase region can be a consequence of E107A–α interactions that are more attractive than HGD–α interactions. A full quantitative analysis of the joint light scattering, tie line, and phase boundary data will require further experimental and theoretical work.

Fig. 3 shows that the liquid–liquid phase boundaries of E107A–α mixtures were lower than those of HGD–α mixtures by about 5 °C. Such a reduction in $T_{ph}$ is exactly what would be expected as the initial response of this system to increased γ–α attraction, based on the work of Stradner, Dorsaz, and coworkers (20, 22), as we now explain. They performed a molecular dynamics (MD) simulation to model their small-angle neutron scattering (SANS) data (20) and applied thermodynamic perturbation theory to study the phase boundaries (21, 22). The γB–α attraction, for which MD simulations were consistent with SANS,

put these mixtures just beyond the lower edge of a stability zone that extends from about 0.5 $k_BT$ to 1.0 $k_BT$ in the γB–α attraction well-depth (20, 22). For those mixtures, initial increases in the γB–α attraction are expected to decrease $T_{ph}$, while rotating tie lines counterclockwise toward density–density-type liquid–liquid phase separation (see figures 6, 10, 11, and 14 in ref. 22 and corresponding discussion). This behavior is consistent with the present data. Further increases in well-depth, on the order of 0.5 $k_BT$ in magnitude, are expected to continue to rotate tie lines and eventually to lead to increased $T_{ph}$ in a composition-dependent manner (22), as we also show with use of a generalized van der Waals free energy model in *Appendix S1*. Because the γB–α mixture phase diagram (21), is quantitatively quite similar to the HGD–α mixture phase diagram found here, the starting values of the interaction parameters for the two systems are likely to be quite similar. Accordingly, we hypothesize that the contrast between the HGD–α and the E107A–α phase diagrams results from the predicted, initially decreased $T_{ph}$ and concomitant enhancement of density-driven phase separation in response to increased γ–α attraction.

Consistent with this hypothesis, we note that in the electrostatic modeling work we found a difference in interaction strengths of approximately 0.4 kcal/mole or 0.7 $k_BT$ that was more attractive for E107A–α than for HGD–α (*Appendix S2*). In view of the fact that angular averaging of patchy interactions as well as nonelectrostatic interactions will also be of relevance, the magnitude of the modeled increase in strength of attractive electrostatic interactions between the HGD–α and the E107A–α cases is quite compatible with the size of approximately 0.5 $k_BT$ predicted by Dorsaz et al. (22) to lead to enhancement of density-type fluctuations.

The decreased $T_{ph}$ in response to increased γ-α attraction in ternary mixtures contrasts with binary protein-water mixtures, in which increased attraction raises $T_{ph}$. The mean-field model in *Appendix S1* shows how such a decrease can occur in ternary mixtures. Thus, in analogy to the fact that increased $T_{ph}$ signals increased homologous attraction in binary aqueous γ-crystallin solutions, the decreased $T_{ph}$ in ternary γ–α mixtures suggests increased γ–α attraction. The measured tie lines (Fig. 4) showed that for HGD–α mixtures, the segregation of the two phases is by protein type and remains so even as the total protein concentration or weight fraction of α-crystallin is increased, consistent with what is found for bovine γB–α mixtures (21).

In contrast, the distinct compositions of the coexisting phases, and the dramatic rotation of the slope of the tie lines for the E107A–α mixture at $X_\alpha = 0.35$ and 0.50 relative to the HGD–α mixtures, strongly suggest a density-type phase separation as a result of the increase in γ–α attraction due to the E107A mutation. Density-type phase separation in response to increased γ–α attraction was predicted in Dorsaz et al. (see especially figures. 10 and 11 and the accompanying text) (22). This is of considerable significance because the protein composition at the central core of the eye lens is such that the amounts of the α- and γ-crystallins are comparable to $X_\alpha = 0.50$. While at $X_\alpha = 0.2$, the paired compositions and the direction of the tie line connecting the coexisting phases at equilibrium are very similar for both HGD–α and E107A–α, the direction of the tie line is already found to be tilted toward the density-type phase separation for the E107A–α mixture at $X_\alpha = 0.35$. This is remarkable because it documents a clear shift in the magnitude of the heterologous protein–protein interactions between α- and γ-crystallins at the molecular level. We hypothesize that the susceptibility of the E107A–α mixture to density-type phase separation can facilitate the formation of density inhomogeneities in the solution well above the phase boundary and also contribute to enhanced light scattering that we have observed, as we explain below.

One of the key reasons that increased E107A–α attraction can contribute to increased light scattering is that enhanced density fluctuations also enhance refractive index fluctuations and thereby scatter more light than other composition fluctuations. A mean-field model that includes a detailed rationale for the linkage between E107A–α attraction and enhanced light scattering is presented in *Appendix S1*. Although other factors detailed there are also of importance, one factor is that increased alignment between the direction of least Gibbs free energy second derivative and that of the index of refraction gradient ($\nabla n$), leads to increased light scattering (29). Therefore in Fig. 4*D*, using published refractive index increments for α-crystallin (34) and γB-crystallin (35), we compare $\nabla n$ with the tie lines, which serve to estimate directions of minimal Gibbs free energy second derivative nearby in the single-phase region, as explained in *Appendix S1*. As shown in Fig. 4 and Fig. S4*II*, the E107A–α tie line directions are approximately 31° from $\nabla n$, while the HGD–α tie lines are 70° from $\nabla n$, qualitatively consistent with the lower intensity observed in HGD–α mixtures, even though they are closer to the phase separation (see *Appendix S1*).

In conclusion, we have presented an intriguing case of a cataract-associated mutant, E107A of human γD-crystallin, which has comparable γ–γ interactions to those in HGD and maintains its structure and stability, similar to the other mutants we reported earlier (8, 12, 13). However, in striking contrast to the other mutants, aqueous solutions of the pure E107A mutant also do not show either a lowered solubility or any indication of the formation of a condensed phase. In fact, the data show a significant alteration in the heterologous interaction of the mutant protein with α-crystallin, relative to the wild type. More precisely, the dramatic rotation in the tie lines connecting coexisting phases in the E107A–α-crystallin mixtures, the altered phase boundary and enhanced light scattering, compared to the HGD–α-crystallin mixtures, are all consistent with increased attractive E107A–α-crystallin interactions. This work thus constitutes an example of a cataract-associated mutant of HGD that shows altered interaction with α-crystallin thereby promoting the thermodynamic instability and opacity observed in cataract formation.

## Materials and Methods

**Cloning, Expression and Purification of Recombinant Proteins.** Overexpression and purification of recombinant wild-type HGD has been reported earlier (8). For the mutant protein, primers were designed and synthesized (MSG Operon) to substitute Glu107 with Ala. Nucleotide sequence in the resulting plasmid was confirmed in-house at the Biomolecular Core facility. Expression and purification of the mutant protein was carried out as for HGD (8). Five independent preparations of HGD and E107A gave an average mass of 20,608 ± 2 and 20,548 ± 1 Da, respectively, using electrospray ionization mass spectrometry (ESIMS), performed at the Center for Functional Genomics at the University at Albany. The results agree with the published mass for HGD (8) and are consistent with the Glu to Ala mutation in HGD.

**Purification of α-crystallin from Young Bovine (Calf) Lenses.** Bovine α-crystallin was extracted from 7 to 10 calf lenses using size-exclusion chromatography (SEC) in a Sepharose CL-6B column (GE Healthcare), and the proteins were eluted isocratically at a flow rate of 2 mL/min using 0.1 M sodium phosphate buffer pH 7, containing 0.02% sodium azide as in (21). The chromatography was repeated two or three times to obtain a single protein peak, which was then characterized by typical spectroscopic criteria.

**Spectroscopic and Static Light-Scattering Studies.** Circular Dichroism (CD) spectra were recorded on a JASCO J-815 spectropolarimeter. Protein concentrations of 0.5 mg/mL in 0.1 M sodium phosphate buffer (pH 7) were used to obtain the near-UV CD spectra in a 10 mm path length cuvette and normalized with respect to protein concentration. Far-UV CD spectra were measured using protein concentrations of 0.1 mg/mL in a 1.0 mm path length cuvette and normalized with respect to the concentration of the backbone peptide bonds.

Tryptophan, Bis-ANS, and Nile Red fluorescence spectra were obtained using a Horiba Jobin Yvon Fluorolog-3 spectrometer. Excitation wavelengths of 290 nm, 390 nm and 540 nm were used to measure tryptophan fluorescence emission, and the fluorescence emission following Bis-ANS and Nile Red binding to the proteins respectively. Excitation and emission slits were

set to 5 nm for all the measurements. Tryptophan fluorescence spectra were measured at a protein concentration of 0.02 mg/mL in 0.1 M phosphate buffer (pH 7) and corrected by subtracting the contribution of buffer. Fluorescence emission following Bis-ANS and Nile Red binding was measured using protein concentrations of 0.1 mg/mL (~5 μM) and a Bis-ANS or Nile Red concentration of 100 μM. Stock solutions of Bis-ANS and Nile Red were prepared in methanol and the final alcohol concentration was maintained below 7% v/v when the reagents were mixed with the proteins. Concentrations of Bis-ANS and Nile Red were measured using extinction coefficients of 16.8 $mM^{-1}\,cm^{-1}$ at 385 nm (36) and 45 $mM^{-1}\,cm^{-1}$ at 552 nm (37), respectively. Spectra were corrected by subtracting the contribution of the buffer containing the appropriate amount of either reagent.

Static light-scattering experiments were performed using a Brookhaven light-scattering model 200SM goniometer and a temperature-controlled sample stage, equipped with a 633 nm laser. Data were collected at a scattering angle of 90°. Protein samples were in the concentrations range of 260–270 mg/mL and Rayleigh ratios were determined as described in ref. 38 using toluene as the standard.

**Thermal and Chemical Denaturation of HGD and E107A.** Thermal stability of HGD and E107A was determined using near-UV CD and monitoring the change in ellipticity at 290 nm as function of temperature. CD spectra were collected at 5 °C intervals from 50 °C to 65 °C and at every 2 °C from 67 °C to 88 °C. Protein samples were equilibrated at each temperature, and each spectrum was an average of four different scans. The midpoint of the thermal denaturation profile gave the melting points ($T_m$) of proteins.

Chemical denaturation due to guanidinium hydrochloride (Gdn.HCl) was monitored using tryptophan fluorescence emission spectra. The concentration of Gdn.HCl was determined using a refractometer (model $r^2$ mini, Reichert). Samples containing increasing concentrations of Gdn.HCl ranging from 0 M to 5.5 M and a final protein concentration of 0.02 mg/mL were used for the fluorescence measurements. Each sample was equilibrated for at least 7 h at 25 °C prior to measurement, and the spectra were corrected for the contribution of the appropriate concentration of Gdn.HCl. The ratio of the fluorescence intensities at 360 nm and 320 nm were used for data analysis.

**Liquid–Liquid Phase Separation-Coexistence Curves and Tie Lines.** $T_{ph}$ measurements were made using the cloud-point method (39), and the coexistence curves for pure HGD and E107A were mapped as described earlier (8). For tie line measurements in solutions of ternary mixtures containing HGD–α and E107A–α, the coexisting liquid phases were formed by quenching the clear mixtures to a temperature below the coexistence curve (21), followed by gentle centrifugation at 1,000 × *g* for 50–70 h in a rotor preequilibrated at the quench temperature. The samples were considered to be at equilibrium when the clouding temperature ($T_{cloud}$ values) of the separated liquid phases were within 1 °C of the centrifugation temperature and also typically within 1 °C of each other. Compositions of the separated liquid phases were determined using SEC.

**Note** See also ref. 40, which further supports our analysis..

**ACKNOWLEDGMENTS.** This work was supported by National Institutes of Health grants EY018249 (G.M.T) and EY010535 (J. Pande). J. Patrosz, a student of the Honors College at University at Albany was supported in part by the University at Albany Summer Research Program and received a Goldwater Scholarship while doing research in the Pande lab.

1. Hejtmancik JF (2008) Congenital cataracts and their molecular genetics. *Semin Cell Dev Biol* 19:134–149.
2. Benedek GB (1971) Theory of transparency of the eye. *Appl Opt* 10:459–473.
3. Delaye M, Tardieu A (1983) Short-range order of crystallin proteins accounts for eye lens transparency. *Nature* 302:415–417.
4. Andley UP (2007) Crystallins in the eye: Function and pathology. *Prog Retin Eye Res* 26:78–98.
5. Aarts HJ, Jacobs EH, van Willigen G, Lubsen NH, Schoenmakers JG (1989) Different evolution rates within the lens-specific beta-crystallin gene family. *J Mol Evol* 28:313–321.
6. Benedek GB (1997) Cataract as a protein condensation disease: The Proctor lecture. *Invest Ophth Vis Sci* 38:1911–1921.
7. Gunton JD, Shiryayev A, Pagan DL (2007) *Protein Condensation: Kinetic Pathways to Crystallization and Disease* (Cambridge Univ Press, Cambridge, UK; New York) p 364.
8. Pande A, et al. (2000) Molecular basis of a progressive juvenile-onset hereditary cataract. *Proc Natl Acad Sci USA* 97:1993–1998.
9. Stephan DA, et al. (1999) Progressive juvenile-onset punctate cataracts caused by mutation of the gammaD-crystallin gene. *Proc Natl Acad Sci USA* 96:1008–1012.
10. Pande A, Gillot D, Pande J (2009) The cataract-associated R14C mutant of human gamma D-crystallin shows a variety of intermolecular disulfide cross-links: A Raman spectroscopic study. *Biochemistry* 48:4937–4945.
11. Kmoch S, et al. (2000) Link between a novel human gammaD-crystallin allele and a unique cataract phenotype explained by protein crystallography. *Hum Mol Genet* 9:1779–1786.
12. Pande A, et al. (2001) Crystal cataracts: human genetic cataract caused by protein crystallization. *Proc Natl Acad Sci USA* 98:6116–6120.
13. Pande A, et al. (2005) Decrease in protein solubility and cataract formation caused by the Pro23 to Thr mutation in human gamma D-crystallin. *Biochemistry* 44:2491–2500.
14. Fu L, Liang JJ (2002) Conformational change and destabilization of cataract gammaC-crystallin T5P mutant. *FEBS Lett* 513:213–216.
15. Pigaga V, Quinlan RA (2006) Lenticular chaperones suppress the aggregation of the cataract-causing mutant T5P gamma C-crystallin. *Exp Cell Res* 312:51–62.
16. Messina-Baas OM, Gonzalez-Huerta LM, Cuevas-Covarrubias SA (2006) Two affected siblings with nuclear cataract associated with a novel missense mutation in the CRYGD gene. *Mol Vis* 12:995–1000.
17. Bera S, Ghosh SK (1998) Interaction of H(+)-ions with alpha-crystallin: Solvent accessibility of ionizable side chains and surface charge. *Biophys Chem* 70:147–160.
18. Bettelheim FA, Chen A (1998) Thermodynamic stability of bovine alpha-crystallin in its interactions with other bovine crystallins. *Int J Biol Macromol* 22:247–252.
19. Takemoto L, Sorensen CM (2008) Protein-protein interactions and lens transparency. *Exp Eye Res* 87:496–501.
20. Stradner A, Foffi G, Dorsaz N, Thurston G, Schurtenberger P (2007) New insight into cataract formation: Enhanced stability through mutual attraction. *Phys Rev Lett* 99:198103.
21. Thurston GM (2006) Liquid-liquid phase separation and static light scattering of concentrated ternary mixtures of bovine alpha and gammaB crystallins. *J Chem Phys* 124:134909.
22. Dorsaz N, Thurston GM, Stradner A, Schurtenberger P, Foffi G (2009) Colloidal characterization and thermodynamic stability of binary eye lens protein mixtures. *J Phys Chem B* 113:1693–1709.
23. Horwitz J (1993) Proctor Lecture. The function of alpha-crystallin. *Invest Ophth Vis Sci* 34:10–22.
24. Veretout F, Tardieu A (1989) The protein concentration gradient within eye lens might originate from constant osmotic pressure coupled to differential interactive properties of crystallins. *Eur Biophys J* 17:61–68.
25. Wang Y, Lomakin A, McManus JJ, Ogun O, Benedek GB (2010) Phase behavior of mixtures of human lens proteins Gamma D and Beta B1. *Proc Natl Acad Sci USA* 107:13282–13287.
26. Evans P, Bateman OA, Slingsby C, Wallace BA (2007) A reference dataset for circular dichroism spectroscopy tailored for the betagamma-crystallin lens proteins. *Exp Eye Res* 84:1001–1008.
27. Mandal K, Bose SK, Chakrabarti B, Siezen RJ (1985) Structure and stability of gamma-crystallins. I. Spectroscopic evaluation of secondary and tertiary structure in solution. *Biochim Biophys Acta* 832:156–164.
28. Pande A, Ghosh KS, Banerjee PR, Pande J (2010) Increase in surface hydrophobicity of the cataract-associated P23T mutant of human gammaD-crystallin is responsible for its dramatically lower, retrograde solubility. *Biochemistry* 49:6122–6129.
29. Ross DS, Thurston GM, Lutzer CV (2008) On a partial differential equation method for determining the free energies and coexisting phase compositions of ternary mixtures from light scattering data. *J Chem Phys* 129:064106.
30. Siezen RJ, Fisch MR, Slingsby C, Benedek GB (1985) Opacification of gamma-crystallin solutions from calf lens in relation to cold cataract formation. *Proc Natl Acad Sci USA* 82:1701–1705.
31. Liu C, et al. (1996) Phase separation in aqueous solutions of lens gamma-crystallins: Special role of gamma s. *Proc Natl Acad Sci USA* 93:377–382.
32. Basak A, et al. (2003) High-resolution X-ray crystal structures of human gammaD crystallin (1.25 A) and the R58H mutant (1.15 A) associated with aculeiform cataract. *J Mol Biol* 328:1137–1147.
33. Laganowsky A, et al. (2010) Crystal structures of truncated alphaA and alphaB crystallins reveal structural mechanisms of polydispersity important for eye lens function. *Protein Sci* 19:1031–1043.
34. Pierscionek B, Smith G, Augusteyn RC (1987) The refractive increments of bovine alpha-, beta-, and gamma-crystallins. *Vision Res* 27:1539–1541.
35. Fine BM (1994) Light scattering by aqueous protein solutions that exhibit liquid-liquid phase separation. PhD thesis (Massachusetts Inst of Technology).
36. Yu XC, Margolin W (1998) Inhibition of assembly of bacterial cell division protein FtsZ by the hydrophobic dye 5,5′-bis-(8-anilino-1-naphthalenesulfonate). *J Biol Chem* 273:10216–10222.
37. Ruvinov SB, et al. (1995) Ligand-mediated changes in the tryptophan synthase indole tunnel probed by nile red fluorescence with wild type, mutant, and chemically modified enzymes. *J Biol Chem* 270:6357–6369.
38. Schurtenberger P, Augusteyn RC (1991) Structural properties of polydisperse biopolymer solutions: A light scattering study of bovine alpha-crystallin. *Biopolymers* 31:1229–1240.
39. Broide ML, Berland CR, Pande J, Ogun OO, Benedek GB (1991) Binary-liquid phase separation of lens protein solutions. *Proc Natl Acad Sci USA* 88:5660–5664.
40. Dorsaz N, Thurston GM, Stradner A, Schurtenberger P, Foffi G (2011) Phase separation in binary eye lens protein mixtures. *Soft Matter* doi:10.1039/C0SM00156B.